Global Potentials for Calcium and Strontium Solids

Jason E. Hearn, Roy L. Johnston[1], Simona Leoni and John N. Murrell

School of Chemistry and Molecular Sciences, University of Sussex, Brighton BN1 9QJ, United Kingdom

Abstract:

Empirical two- plus three-body potentials have been derived for calcium and strontium, and applied to the fcc and bcc structures of both metals. The parameters are derived by fitting phonon frequencies, elastic constants and other structural data. The potentials obtained give a sensible ordering of solid structures, and good energy profiles along the (Bain) tetragonal distortion pathway between the fcc and bcc allotropes. The potentials have been used to calculate the fcc and bcc phonon densities of states (DOS), from which the Helmholtz free energies and the fcc $\rightarrow$ bcc transition temperatures (T_c) have been evaluated. We overestimate the value of T_c for Ca and underestimate it for Sr. The potentials give surface energies which are in good agreement with experiment.

[1]Present address: School of Chemistry, University of Birmingham, Edgbaston, Birmingham, B15 2TT, United Kingdom

1 Introduction: phase transitions of the alkaline earth metals

The alkaline earth (Group II) metals are known to adopt one of three structures : hexagonal close packed (hcp); face centred cubic (fcc); or body centred cubic (bcc), depending on temperature and pressure [1]. For a given set of conditions the most stable phase is that having the lowest chemical potential. To evaluate this, it is necessary to have an expression for the potential energy of the crystal which can be used to calculate phonon frequencies and the density of (phonon) states (DOS). Group II metals are a good choice for looking at this problem, as they exhibit more than one crystalline phase whose phonon and elastic properties have been studied. Any empirical potential, for which global accuracy is desired, must be able to describe all such structures as well as performing sensibly for any structures which may not have been observed to date.

The ground state structures and temperature- and pressure-induced phase transitions of the group II metals are summarized in Table 1. The theoretical sequence of phase transitions (at constant pressure) is hcp $\rightarrow$ fcc $\rightarrow$ bcc $\rightarrow$ hcp [2]. This pattern is revealed on descending the group, with Be and Mg adopting the hcp structure at low and ambient temperatures, while Ca and Sr have the fcc structure, and Ba and Ra are bcc. At atmospheric pressure, Beryllium undergoes a hcp $\rightarrow$ bcc phase transition at a critical temperature (T_c) of 1523 K, just below the melting point (T_m = 1563 K) whilst Mg melts at 922 K without undergoing any phase transition at atmospheric pressure. At room temperature, however, Mg transforms to bcc at a pressure of 50 GPa. Ca undergoes a fcc $\rightarrow$ bcc transition at 721 K (1 atm) or 19.7 GPa (room temperature). The earlier suggestion of an intermediate hcp phase has been attributed to the presence of hydrogen atom impurities. Strontium transforms from fcc to bcc at around 830 K (again with a reported intermediate hcp form probably being due to H impurities), or at 3.8 GPa (room temperature). Barium has a stable bcc structure from 5 K to the melting point (1002K) only transforming to the hcp phase at high pressure (5.3 GPa). Only the bcc structure is known for radium.

In an earlier paper by Andersson, Johnston and Murrell (AJM) [3] on Ca, a potential was found which fitted phonon dispersion curves of both the fcc and bcc structures very well. The potential also gave the correct ordering of other hypothetical solid structures, and gave a realistic description of the fcc $\rightarrow$ bcc pathway. The potential was applied to clusters and was found to favour icosahedral structures.

The aim of the present work is to derive a potential for Sr and an improved potential for Ca. These potentials will be tested for their ability to reproduce the experimental phonon DOS, and (via the calculation of the Helmholtz free energy) the fcc $\rightarrow$ bcc transition temperature.

2 The potential

Pairwise additive (central) forces do not give a good description of bonding in metals, and this has led to studies of many-body forces for describing metallic cohesion. Several of these are known collectively as 'glue models' [4], and include the EAM (embedded atom method) of Daw and Baskes [5], the EMT (effective medium theory) of Norskøv [6], the FS (Finnis Sinclair) N-body potentials [7], and the long range FS potentials of Sutton and Chen [8], all of which have proved reasonably successful in reproducing experimental properties. Specific potentials which have been derived for the alkaline earth metals include: the volume dependent pseudopotentials of Moriarty [9]; Wang and Overhauser [10]; and Singh and Singh (who derived potentials for both the fcc and bcc allotropes of Ca and Sr) [11]. In this paper we use an alternative potential by Murrell and Mottram (MM) which has been shown to be applicable to simple metals, transition metals and semiconductors.

Our objective has been to obtain a many-body potential energy function which is able to reproduce physical properties of the crystalline solid, and subsequently to examine the structural and dynamical aspects of solids, liquids surfaces and clusters. Underlying this approach is the assumption that such potentials will not have a strong temperature dependence.

The MM potential that we have used [12, 13, 14, 15] consists of two-body and three-body components, with the two-body term expressed as a reduced variable Rydberg function [14] as follows:

$$V_{ij}^{(2)}/D = -(1 + a_2\rho_{ij})exp(-a_2\rho_{ij}) \tag{1}$$

where

$$\rho_{ij} = \frac{(r_{ij} - r_e)}{r_e} \tag{2}$$

D and r_e are scaling factors so that the lattice (cohesive) energy and lattice constant for the reference structure (in our case the fcc ground state structure) can be reproduced exactly. The three-body term is represented by

$$V_{ijk}^{(3)} = D\mathbf{P}(Q_1, Q_2, Q_3)\mathbf{F}(a_3, Q_1) \tag{3}$$

where the function $\mathbf{P}$ is a polynomial in the symmetry co-ordinates, Q_i for a triangle with sides ρ_{ij}:

$$\begin{pmatrix} Q_1 \\ Q_2 \\ Q_3 \end{pmatrix} = \begin{pmatrix} \sqrt{1/3} & \sqrt{1/3} & \sqrt{1/3} \\ 0 & \sqrt{1/2} & -\sqrt{1/2} \\ \sqrt{2/3} & -\sqrt{1/6} & -\sqrt{1/6} \end{pmatrix} \begin{pmatrix} \rho_{ij} \\ \rho_{ik} \\ \rho_{jk} \end{pmatrix} \tag{4}$$

The function $\mathbf{F}$ is the damping function for the three- body term, the form of which will be described in greater detail below. The coefficients of $\mathbf{P}$ are optimised to experimental data for selected values of a_2 and a_3 by means of a least squares routine. The following quartic form for the polynomial $\mathbf{P}$ is totally symmetric to exchange of like atoms :

$$\begin{aligned}\mathbf{P}(Q_1,Q_2,Q_3) &= c_0 + c_1Q_1 + c_2Q_1^2 + c3(Q_2^2+Q_3^2) + c_4Q_1^3 + \\ &\quad c_5Q_1(Q_2^2+Q_3^2) + c_6(Q_3^3 - 3Q_3Q_2^2) + c_7Q_1^4 + \\ &\quad c_8Q_1^2(Q_2^2+Q_3^2) + c_9(Q_2^2+Q_3^2)^2 + c_{10}Q_1(Q_3^3 - 3Q_3Q_2^2)\end{aligned} \tag{5}$$

The damping function $\mathbf{F}$ (3) must decay exponentially at large values of the perimeter of the triangle to counter the growth of the polynomial term. Several damping functions, with differing short range behaviour, have been investigated :

$$\mathbf{F} = exp(-a_3Q_1) \tag{6}$$

$$\mathbf{F} = \frac{1}{2}(1 - tanh(\frac{a_3Q_1}{2})) \tag{7}$$

$$\mathbf{F} = sech(a_3Q_1) \tag{8}$$

3 Data used in potential optimisation

The majority of the data used in our optimisations are from phonon dispersion measurements. For calcium, dispersion curves for the ground state fcc structure have been determined by Stassis *et al.* by single-crystal inelastic neutron scattering at 300K [16]. We have used a total of 14 frequencies for the fcc structure along the high symmetry lines [100], [110], and [111]. All phonon frequencies are squared, multiplied by the atomic mass and divided by the lattice spacing to give a quantity with the same dimensions as the elastic constants. For consistency, the elastic constants published by Stassis *et al.* were also used. These were obtained from an 8-neighbour Born-von

Kármán (BvK) fit to the phonon dispersion curves. For the bcc structure, tabulated phonon frequencies do not exist, and so we reproduced them from their published force constants, obtained from a 3-neighbour axially symmetric BvK fit to the experimental polycrystalline neutron time-of-flight data [17] at 726K, i.e. just above the transition temperature of 721K [18]. Heiroth *et al.* also provide elastic and force constants for the fcc structure, but for consistency with the phonon frequency data, the elastic constants from Stassis *et al.* were preferred. The elastic constants for Ca are listed in Table 2.

For strontium, the fcc phonon dispersion curves were taken from the 293 K results of Buchenau *et al.*, who give a 3 shell BvK fit [19]. The phonon curves were again reproduced from these force constants to provide the 'experimental' data for our fitting routine. For the bcc structure, Mizuki and Stassis measured the single crystal phonon dispersion curves [20], and performed a 7-neighbour BvK fit to the experimental data. Frequencies calculated from the resulting force constants were used as input to our program. The elastic constants for fcc Sr were calculated from Buchenau's force constants, to give: $C_{11} = 0.1532$, $C_{12} = 0.1042$ and $C_{44} = 0.1002$. For the bcc structure there is considerable doubt as to the true elastic constants, as can be seen in Table 2. In particular, the force constants published by Mizuki and Stassis [20] give a negative value for C_{12} and predict that C_{44} is greater than C_{11}. This pattern of elastic constants is incompatible with those of bcc Ca and Ba [9] and is also at variance with those quoted by Singh and Singh [11]. We have, therefore, adopted the 'experimental' values of Singh and Singh for our data set.

In our previous study [3], we used an estimated vacancy energy of 0.5 eV for Ca as there is no experimental value available. There is also no experimental vacancy energy available for Sr. In the present study, the vacancy energies for both ground state structures were taken from Ziesche *et al.* who studied monovacancies in simple metals described by the jellium model [21].

The values of E_{vac} that we have adopted are the unrelaxed vacancy formation energies (0.70 eV for Ca and 0.66 eV for Sr) quoted by Ziesche. These values agree with the results of self consistent calculations reported by Ziesche in an earlier paper [22]. It should be noted that the calculated relaxed vacancy energies are significantly lower (0.37 eV or 0.33 eV for Ca [23]) than the unrelaxed values, but it is computationally more economical to calculate the unrelaxed energies. The vacancy energies of the bcc allotropes are also unknown, but these are not required in our fitting procedure.

The ground state lattice spacings [18] and cohesive energies [24] for the fcc structures are fitted exactly in our procedure by appropriate choice of the D and r_e scaling factors. For Ca, we also add the bcc lattice spacing to our least squares data. This was introduced in an attempt to provide a Ca potential with a larger bcc lattice spacing; the AJM potential underestimates r_l (bcc), leading to the incorrect prediction that bcc Ca is more dense than fcc. As the strontium potential gives the correct ordering of bcc and fcc densities, the lattice spacing of the bcc structure was not used in the fitting procedure. Preliminary calculations on Sr, however, greatly underestimated the difference in cohesive energy between fcc and bcc and to rectify this we included an fcc-bcc difference of 0.034 eV in our least squares data as this value was predicted to give a good transition temperature between the two structures (*vide infra*).

We have in total an 18 point least squares data set for each structure, with all the points having an equal weighting of 1 (with the exception of the bcc-fcc cohesive energy difference for Sr which was given a higher weighting of 3) in the least squares optimisation procedure. These data are summarised in Table 3 for both elements.

4 Potentials and lattice dynamics.

A thorough search was carried out in a_2 and a_3 space, in order to find potentials which can simultaneously fit the experimental data for both the fcc and the bcc structures of Ca and Sr while maintaining a sensible order of cohesive energies of 3, 2 and 1-dimensional lattices. The potentials were also checked to ensure that they do not collapse at short range. The best potential obtained for Ca has a hyperbolic tangent three-body damping term (7) . The AJM potential for Ca was based on the exponential damping function, but this gave poorer fits to the low frequency phonon data than we have now achieved. This feature is important in calculating the transition temperature. For Sr, it was found that the sech (8) function was found to be a little better than the tanh. These potentials are presented in Table 4

The calculated phonon curves for fcc and bcc Ca along high symmetry lines in the Brillouin Zone are compared with experiment in Figure 1. The agreement is excellent for both structures. We are able to calculate 'experimental' phonon frequencies over the whole of **q** space for either structure, by using the force constants published by Stassis *et al.* (fcc) [17] and Heiroth *et al.* (bcc) [11]. The values deduced from our potential agree well with those, having a a maximum error of 0.4 THz (underestimated), at the highest frequency modes for fcc over the whole of q-space. Along high symmetry lines however, the largest error is at **q**=[1,0,0] for the bcc structure. For fcc and bcc Ca, our frequencies are significantly better than those calculated from the pseudopotential of Singh and Singh [11], They are also better than Moriarty's calculations on fcc Ca [9], and comparable to those of Wang and Overhauser [10] and Li and Goddard (using their interstitial electron model) [25]. The fit to the phonons are as good as direct (unconstrained by an underlying potential) BvK fits of Stassis [17], Heiroth [11] and Ghorai [23]. Phonon curves for Sr are shown in Figure 2.

The calculated phonon frequencies for fcc Sr are in very good agreement with the experimental data of Buchenau *et al.*. The fit to the bcc experimental data is also on the whole very good, with only a slight underestimation of the T1 mode by 0.5 THz at [0.5,0.5,0]. Like Singh and Singh, we get a crossover in the [q00] direction between the L and T modes, contrary to experimental evidence, though the experimental curves are in fact very close to each other [20].

As stated above, there is some doubt as to the best values of the elastic constants of both Ca and Sr. For Ca, we predict the correct ordering of elastic constants for both fcc and bcc structures. For bcc, our value of C_{44} is much smaller than the value of Singh and Singh [11] but is comparable to that of Heiroth *et al.* [17]. For Sr, we achieve good agreement with the experimental values for the fcc structure and although we disagree on the ordering of C_{12} and C_{44}, the difference between these is very small. For the bcc structure, the correct ordering (according to Singh and Singh [11]) is obtained and there is good agreement with the experimental values of C_{11} and C_{44}. The least satisfactory result from our potential is that for Ca the bcc lattice spacing is still too low by 0.112 Å) [18]. This is not much of an improvement on our previous work (AJM) and gives bcc a more dense structure than fcc, contrary to experiment. The calculated volume per atom for bcc is 41.73 Å^3 and the experimental value is 44.96 Å^3. For Sr, on the other hand, we correctly calculate the bcc structure to be less dense than fcc, and we slightly overestimate the bcc volume (calculated = 63.55 Å^3; experimental = 57.04 Å^3) [18].

5 Predictions for other bulk structures and surfaces

To show that our potentials give realistic results for a wide range of geometries and coordination numbers, we have calculated cohesive energies and nearest neighbour distances for a number of infinite 1,2 and 3-dimensional structures. This set of structures have been used as tests for potentials by others [14, 26]. The results are listed in Table 5.

The value of E_{coh}(fcc)-E_{coh}(bcc) = 0.015 eV for Ca is consistent with the calculations of Moriarty, who quotes values ranging from 0.013 eV to 0.024 eV [9] and Skriver, who cites a value of 0.024eV using the Linear Muffin-Tin Orbital method [27, 28]. Our calculations give essentially the same cohesive energy for the hcp and fcc structures, while Moriarty and Skriver calculate fcc-hcp energy differences ranging from -0.004 eV to 0.012 eV. For the other structures, the cohesive energy becomes smaller as the coordination number decreases due to the dominance of the two-body part of the potential.

For Sr, Skriver has calculated the fcc structure to be more stable than bcc by 0.011eV and he has calculated a fcc-hcp difference of 0.007eV [28]. Moriarty gives values of 0.024eV and 0.007eV respectively for the fcc-bcc and fcc-hcp gaps respectively [9]. Our calculated fcc-bcc difference (0.013 eV) is in good agreement with Skriver, but we calculate hcp to be slightly more stable than fcc (by -0.002eV). It should be noted that the calculations of Singh and Singh incorrectly predict bcc to be more stable than fcc for both Ca and Sr.[11].

For both metals the cohesive energies of the 2-layer 2-dimensional fcc slabs are in the order f111 > f100 > f110 as expected for an fcc metal, where the decreasing stability of the low index surfaces reflects the decreasing coordination of the surface atoms.

To test how well our potentials reproduce the surface energies of Ca and Sr, calculations have been performed using a model two-sided slab with translational symmetry in the x and y directions. The surface supercell dimensions are such that the x, y and z lengths are all greater than twice the cutoff radius of the potential. This is to ensure that atoms in the centre layer are bulk like (i.e. they do not experience the slab surface) and that there is no intracell correlation of atomic positions. The surfaces are relaxed by allowing movement of entire layers in the z direction. Further details on the model and algorithms used in these calculations can be found elsewhere [29, 30].

In these slab calculations, the surface energy is calculated from :

$$E_s = \frac{-(V - NE_{coh)}}{2A} \tag{9}$$

where V is the total potential energy of the slab, E_{coh} is the bulk cohesive energy, N is the number of atoms in the slab supercell, and A is the surface area of one side of the slab. The calculated (relaxed) surface energies for the low index high symmetry surfaces of fcc and bcc Ca and Sr are listed in Table 6, together with experimental measurements [31] and previously calculated values [33, 32]. Lower surface energies correspond to more stable surfaces.

For the fcc surfaces of both metals, our results are in excellent agreement with experiment. The calculations confirm the predicted stability order (111) > (100) > (110). For the bcc surfaces the stability order (110) > (100) again reflects the coordination number of the surface atoms (the bcc (111) surface has low surface atom coordination and therefore a high surface energy). The experimental values listed by Miedema and coworkers [31, 32] are based on surface tension measurements on the molten metals and probably represent average surface energies. Our values slightly underestimate E_s but are much closer to experiment than are the *ab initio* LMTO calculations of Skriver and Rosengaard [33]. This means that our values for bcc Ca (where no experimental values are yet available) are likely to be more accurate than Skriver's.

Finally, we have also calculated the energies of the (1x2) reconstructed (110) surfaces, for both metals, and found these to be higher than the unreconstructed (110) surfaces. Our potentials therefore predict that, for Ca and Sr, the (110) surfaces are stable with respect to missing-row reconstructions. We are unaware of any experimental data or calculations against which to test this prediction.

6 The Bain path for fcc-bcc interconversion

As our potentials for calcium and strontium give fcc and bcc as stable structures (minima on the potential energy surface), we are able to consider pathways that can interconvert the two. A large number of diffusionless transformations can in theory give this interconversion [34] Here, we study the tetragonal Bain deformation which interconverts fcc and bcc via an intermediate body-centred tetragonal (bct) structure. This pathway involves the minimum of atomic movement and hence minimum strain in the lattice.

Figure 3 shows the bct cell (shaded atoms) and the larger face tetragonal (fct) cell (indicated by the dotted lines) which is rotated by 45^o with respect to the bct cell. In the bct definition, bcc occurs when $c/a = 1.0$, and fcc, when $c/a = \sqrt{2}$ [35]. Thus to convert fcc to bcc we contract parallel to the c axis whilst expanding parallel to the equivalent a and b axes.

The variation of cohesive energy (E) with c/a ratio, along the tetragonal Bain path, is shown in Figure 4, for both Ca and Sr (further details of this calculation can be found in AJM [3]). We have investigated c/a in the range 0.8-1.6 and find two minima, at $c/a = 1$ and $c/a = \sqrt{2}$) corresponding to the bcc and fcc structures respectively. Our calculations predict an activation energy for the fcc $\rightarrow$ bcc transition of 0.0167 eV and 0.0146 eV for Ca and

Sr respectively, and an activation energy in the reverse direction of 0.0014 eV and 0.0018 eV respectively.

Figure 5 shows contour diagrams of cohesive energy plotted against the reduced volume V/V_o (where V_o is the atomic volume of the stable fcc phase) and the c/a ratio. The Figure shows that, for both Ca and Sr, only two minima are found along the Bain path. It is known, however, that other potentials (for different elements) can give rise to metastable bct structures on this potential energy surface [29], [36]. As mentioned above, for Ca, the bcc structure is predicted to have a higher density than the fcc structure ($V/V_0 < 1$), which is contrary to experimental evidence. For Sr, however, we predict the correct ordering of densities, (i.e. $V(bcc)/V_0 > 1$).

7 Phonon densities of states

It has been shown that our potentials for Ca and Sr yield results which are in good agreement with experimental bulk properties of both the fcc and bcc solids. In particular, there is an excellent fit to the experimental phonon dispersion curves. To calculate the thermodynamic stabilities of the two phases and the transition temperature (T_c) it is neccessary to calculate the phonon density of states (DOS) to a high degree of accuracy. DOS curves, as a function of phonon frequency, were obtained by tetrahedral interpolation over a mesh of 17x17x17 points (fcc) or 21x21x21 points (bcc) in the irreducible wedge ($\frac{1}{48}$th) of the Brillouin Zone [37]. The resulting DOS curves are shown in Figures 6 and 7. The DOS is greater for bcc than for fcc in the low frequency region, but is lower for most frequencies above 2.2THz (Ca) or 1.0THz (Sr).

Our DOS calculations for bcc Ca and are in very good agreement with those calculated by Heiroth [17], from a 3-neighbour BvK fit to experimental phonon data. For fcc Ca, however, we have found some incompatibility between the DOS published by Stassis, and his force constants. We are, however, in good agreement with Heiroth's 3-neighbour BvK DOS, although we underestimate the highest frequency by about 0.5 THz. This is consistent with our underestimation of the fcc phonon curves at these high frequencies.

8 Thermodynamics of the fcc-bcc transition

The observed critical temperatures for the fcc $\rightarrow$ bcc phase transitions of Ca and Sr (at 1 atm.) are 721 K and 830 K respectively. The transition temperature T_c is defined as the temperature at which there is no difference in free energy between the two phases. In common with previous work [38, 39], we have calculated the Helmholtz (constant volume) free energy:

$$A(V,T) = U - TS \tag{10}$$

as this quantity is easier to obtain than the Gibbs free energy ($G(P,T) = A + PV$) and, for solids at ambient pressures, the two quantities differ very little.

The largest contributions to the internal energy U are the cohesive energy and the average zero point energy. The latter is given by:

$$\frac{1}{Q}\sum_{j,q}\frac{h\nu_j(q)}{2} \tag{11}$$

where j=1-3 identifies the phonon branches and Q is the total number of **q** points (including weighting factors) used in averaging over the Brillouin Zone (BZ). For this calculation, a uniform mesh (in the irreducible wedge of the BZ) of **q** points was taken; 3541 points for fcc and 8923 for bcc. The difference in the number of points used for fcc and bcc reflects the different shapes of the BZs for these two structures. The calculated average zero point energies are: for Ca 0.0202 eV (fcc) and 0.0196 eV (bcc); and for Sr 0.0130 eV (fcc) and 0.0111 eV (bcc). The lower values for bcc, in both cases, are consistent with the DOS plots shown in Figures 6 and 7, from which it can be seen that the average frequencies are lower for the bcc than the fcc structures.

Within the quasi-harmonic approximation, the temperature dependence of A comes from the entropic contribution due to thermal population of excited states of the phonon modes. This vibrational entropy is given by the following BZ average:

$$\frac{1}{Q}\sum_{j,q} k_B ln[1 - exp(-h\nu_j(q)/k_B T)] \tag{12}$$

Taking the same mesh of **q** points, the calculated vibrational entropies, as a function of temperature, are shown in Figure 8. For both Ca and Sr, we see that the entropy contribution favours the bcc structure at high temperatures. This is because the metastable bcc phase has a large number of low energy (soft) phonon modes [40], as can be seen in Figures 6 and 7.

Using our potentials to calculate ΔA ($= A(bcc) - A(fcc)$) as a function of temperature, we calculate T_c values of 961 K for Ca and 262 K for Sr. These should be compared with the experimental values of 721 K (Ca) and 830 K (Sr). Since our fitting of the phonon frequencies is very good, the deviation from experiment is principally due to over/under-estimating the differences in internal energies of the fcc and bcc metals ($\Delta U = U(bcc) - U(fcc)$). The experimental T_c of 721 K for Ca implies a ΔU value of 0.011 eV. Our calculated value for ΔU (0.014 eV) is slightly greater than this, which is why we overestimate T_c for Ca (by 240 K). For Sr the observed T_c is 830 K which yields, $\Delta U = 0.039$ eV. Our calculated value (0.011 eV) is lower than this, which explains why we underestimate T_c for Sr by a considerable margin (568 K).

In conclusion, our calculated transition temperatures (961 K for Ca and 262 K for Sr) do not agree closely with experiment, but we have shown that only relatively small changes in ΔU are required to give the correct T_c values. Our potentials have not been fitted to precise relative values of the fcc and bcc cohesive energies because these are not well known. It should be noted, however, that in the case of Sr, the ΔU value of 0.039 eV is significantly larger than the values calculated by either Moriarty [27] or Skriver [28]. It is therefore possible that some other factor (such as a breakdown of the quasi-harmonic approximation, wherein the phonon frequencies are assumed to be temperature independent) may be contributing to our error for Sr. In the circumstances, therefore, our results are qualitatively satisfactory.

9 Conclusions

In this paper we have shown that it is possible to derive empirical two- plus three-body potentials for calcium and strontium by simultaneously fitting lattice dynamical properties of the fcc and bcc structures. In both cases the potential gives a very good fit to the high symmetry phonon frequencies and to elastic constant data. A sensible ordering of the cohesive energies of a number of 1-, 2- and 3-D structures is also achieved. Our potentials produce the correct stability ordering for the low index surfaces of the fcc and the bcc allotropes, with surface energies (in good agreement with experiment) in the order (111) $<$ (100) $<$ (110) for fcc and (110) $<$ (100) for bcc. The (110) surfaces of the fcc metals are predicted to be stable with respect to missing row reconstructions.

We are able to reproduce a smooth fcc $\leftrightarrow$ bcc interconversion along the Bain deformation pathway. Our potentials also give good agreement with the experimental phonon densities of states. The potentials have been used to calculate thermodynamic properties and to obtain fcc-bcc transition temperatures for Ca and Sr, but the latter have been shown to be very sensitive to the difference in cohesive energy between the two structures.

The success of our potentials for Ca and Sr, over a wide range of structures, coordination numbers and local geometries, leads us to believe that they should be applicable to the study of the structures, dynamics and thermodynamics of solids, surfaces and clusters of these elements. Studies are currently under way, using these potentials to simulate surface and bulk melting as well as cluster growth.

Acknowledgements

RLJ thanks the Royal Society for a University Research Fellowship (1989-95). SL was visiting the University of Sussex as an ERASMUS student from the University of Bologna, Italy.

References

[1] J. Donohue, *The Structures of the Elements*, 2nd Ed. (Wiley, New York, 1974).

[2] H.L. Skriver Phys. Rev. B, **31**, 1909 (1985).

[3] K.M. Andersson, R.L. Johnston, J.N. Murrell Phys. Rev. B, **49**, 3089 (1994).

[4] F. Ercolessi, E. Tosatti, M. Parinello Phys. Rev. Lett., **57** 719 (1986).

[5] M.S. Daw, M.I. Baskes Phys. Rev. B, **29** 6443 (1984).

[6] J.K. Norskøv Phys. Rev. B, **26** 2875 (1982).

[7] M.W. Finnis, J.E.Sinclair Philos. Mag. A, **50** 45 (1984).

[8] A.P. Sutton, J. Chen Philos. Mag. Lett., **61** 39 (1990).

[9] J.A. Moriarty Phys. Rev. B, **34**, 6738 (1986).

[10] Y.R. Wang, A.W. Overhauser Phys. Rev. B, **35**, 497 (1987).

[11] N. Singh, S. Singh Phys. Stat. Sol. B, **158**, 433 (1990).

[12] J.N. Murrell, R.E. Mottram Mol. Phys., **69**, 571 (1990).

[13] J.N. Murrell, J.A. Rodriguez-Ruiz Mol. Phys., **71**, 823 (1990).

[14] R.L. Johnston, J.-Y. Fang J. Chem. Phys, **97**, 7809 (1992).

[15] J.-Y. Fang, R.L. Johnston, J.N. Murrell Mol. Phys., **78**, 1405 (1993).

[16] C. Stassis, J. Zaretsky, D.K. Misemer, H.L. Skriver, B.N. Harmon Phys. Rev. B, **27**, 3303 (1983).

[17] M. Heiroth, U. Buchenau, H.R. Schober Phys. Rev. B, **34**, 6681 (1986).

[18] W.B. Pearson *Handbook of Lattice Spacings and Structures of Metals and Alloys* (Pergamon, New York, 1958).

[19] U. Buchenau, M. Heiroth, H.R. Schober, J. Evers, G. Oehlinger Phys. Rev. B, **30**, 3502 (1984).

[20] J. Mizuki, C. Stassis Phys. Rev. B, **32**, 8372 (1985).

[21] P. Ziesche, J.P. Perdew, C. Fiolhais Phys. Rev. B, **49**, 7916 (1994).

[22] P. Ziesche, M.J. Puska, T. Korhonen, R.M. Neiminen J. Phys Condens. Matter, **5** 9049 (1993).

[23] A. Ghorai Phys. Stat. Sol. B, **167**, 551 (1991).

[24] C. Kittel *Introduction to Solid State Physics*, 6th ed. (Wiley, New York (1986).

[25] M. Li, W.A. Goddard J. Chem. Phys., **98**, 7995 (1993).

[26] I.J. Robertson, M.C. Payne, V. Heine Europhys. Lett, **15** 301 (1991).

[27] J.A. Moriarty Phys. Rev. B, **16**, 2537 (1977); Phys. Rev. B, **26**, 1754 (1982).

[28] H.L. Skriver Phys. Rev. Lett., **49**, 1768 (1982).

[29] J. Uppenbrink, R.L. Johnston, J.N. Murrell Surf. Sci., **304**, 223 (1994).

[30] H. Cox, R.L. Johnston, J.N. Murrell (in preparation).

[31] A.R. Miedema Z. Metall., **69**, 287 (1978).

[32] F.R. deBoer, R. Boom, W.C.M. Mattens, A.R. Miedema, A.K. Niessen *Cohesion in Metals* (North-Holland, Amsterdam 1988).

[33] H.L. Skriver, N.M. Rosengard Phys. Rev. B, **46**, 7157 (1992).

[34] D.A. Porter, K.E. Easterling *Phase Transformations in Metals and Alloys 2nd Ed*, (Chapman and Hall, London 1992).

[35] E.C. Bain Trans. AIME **70**, 25 (1924).

[36] I.A. Morrison, M.H. Kang, E.J. Mele Phys. Rev. B **39**, 1575 (1989). Phys. Stat. Sol. B **54**, 469 (1972).

[37] G. Lehman, M. Taut Phys. Stat. Sol. B **54**, 469 (1972).

[38] N.L. Allen, M. Braithwaite, D.L. Cooper, W.C. Mackrodt, B. Petch J. Chem. Soc., Faraday Trans. **89**, 4369 (1993).

[39] K.D. Heath, W.C. Mackrodt, V.R. Saunders, M. Causà J. Mat. Chem. **4**, 825 (1994).

[40] P.K. Lam, M.Y. Chou, M.L. Cohen J. Phys. C **17**, 2065 (1984).

Figure Captions

Figure 1: Phonon dispersion curves calculated for fcc and bcc Ca along high symmetry directions. Experimental data are represented by circles and triangles.

Figure 2: Phonon dispersion curves calculated for fcc and bcc Sr along high symmetry directions. Experimental data are represented by circles and triangles

Figure 3: Definition of bct (shaded atoms) and fct (dotted lines) unit cells.

Figure 4: Variation of cohesive energy (E) with c/a ratio, along the Bain deformation path, for Ca and Sr.

Figure 5: Contour plots of the potential-energy surface for centred tetragonal Ca and Sr as a function of c/a and the reduced volume V/V_0. The contour spacing in both cases is 0.003 eV.

Figure 6: Phonon DOS for fcc and bcc Ca. The dotted lines represent the DOS calculated from experimental force constants.

Figure 7: Phonon DOS for fcc and bcc Ca. The dotted lines represent the DOS calculated from experimental force constants.

Figure 8: Variation of vibrational entropy with temperature for fcc and bcc Ca and Sr.

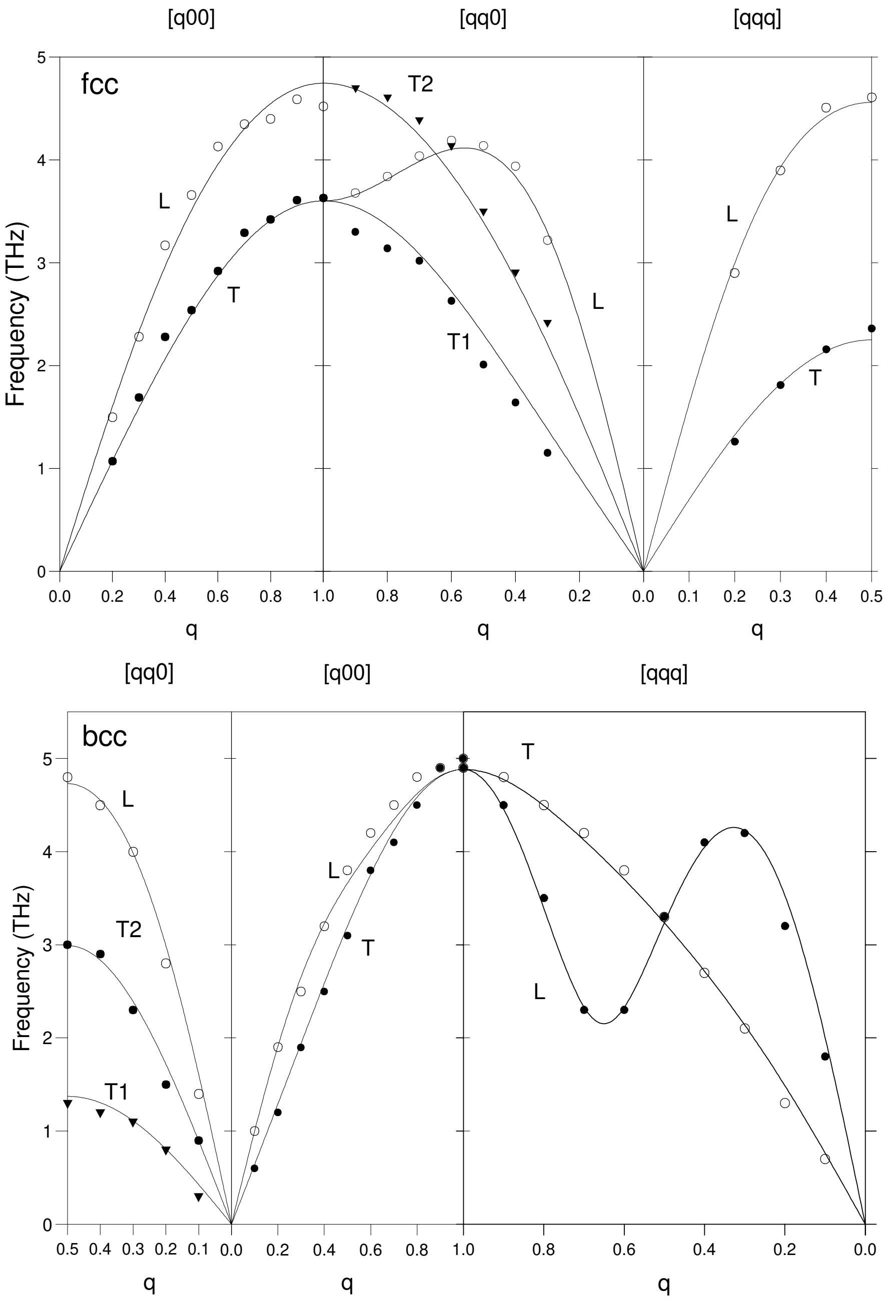

Figure 1: Phonon dispersion curves calculated for fcc and bcc Ca along high symmetry directions. Experimental data are represented by circles and triangles

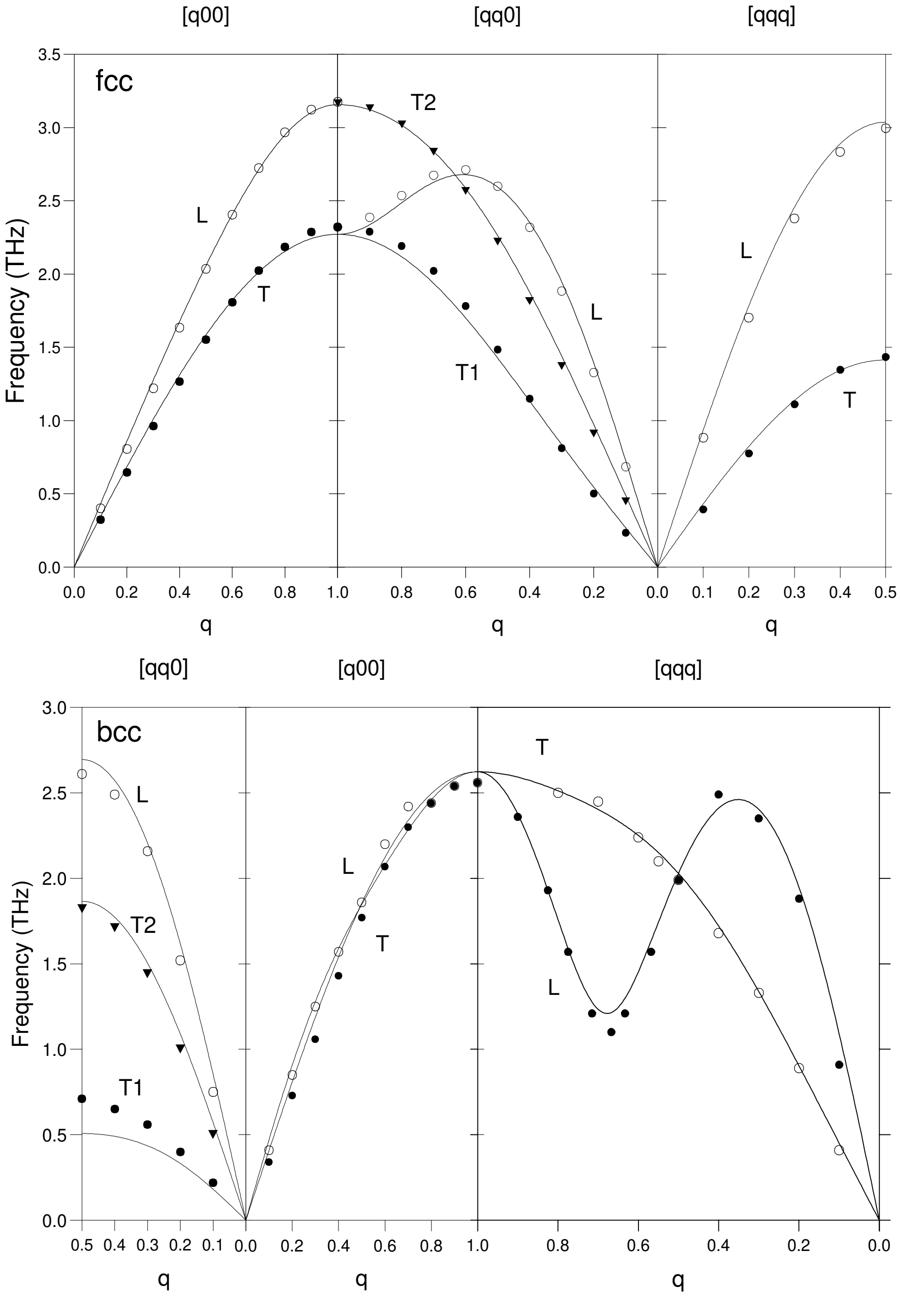

Figure 2: Phonon dispersion curves calculated for fcc and bcc Sr along high symmetry directions. Experimental data are represented by circles and triangles

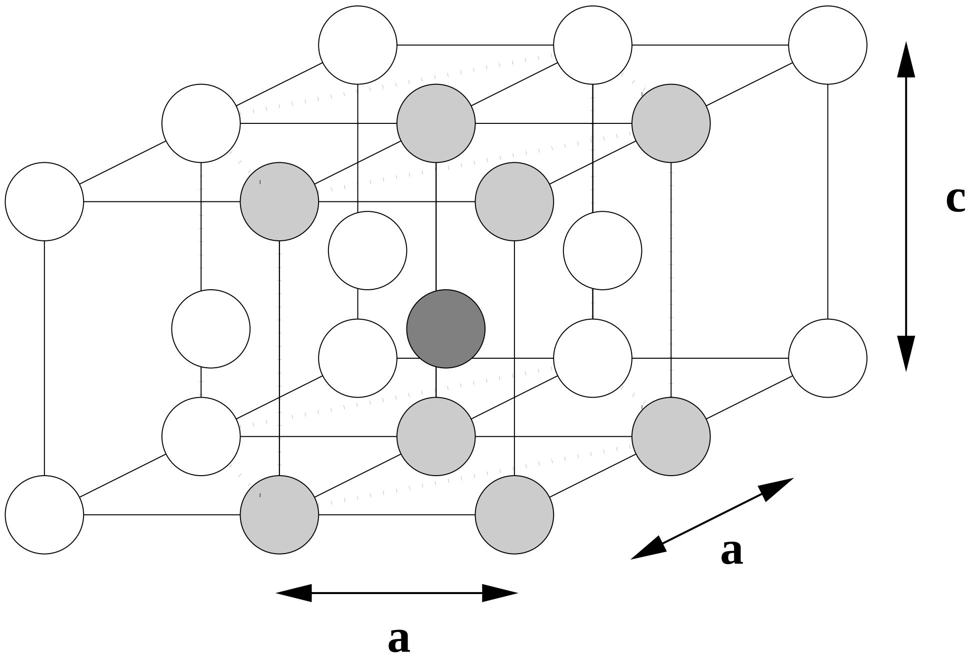

Figure 3: Definition of bct (shaded atoms) and fct (dotted lines) unit cells.

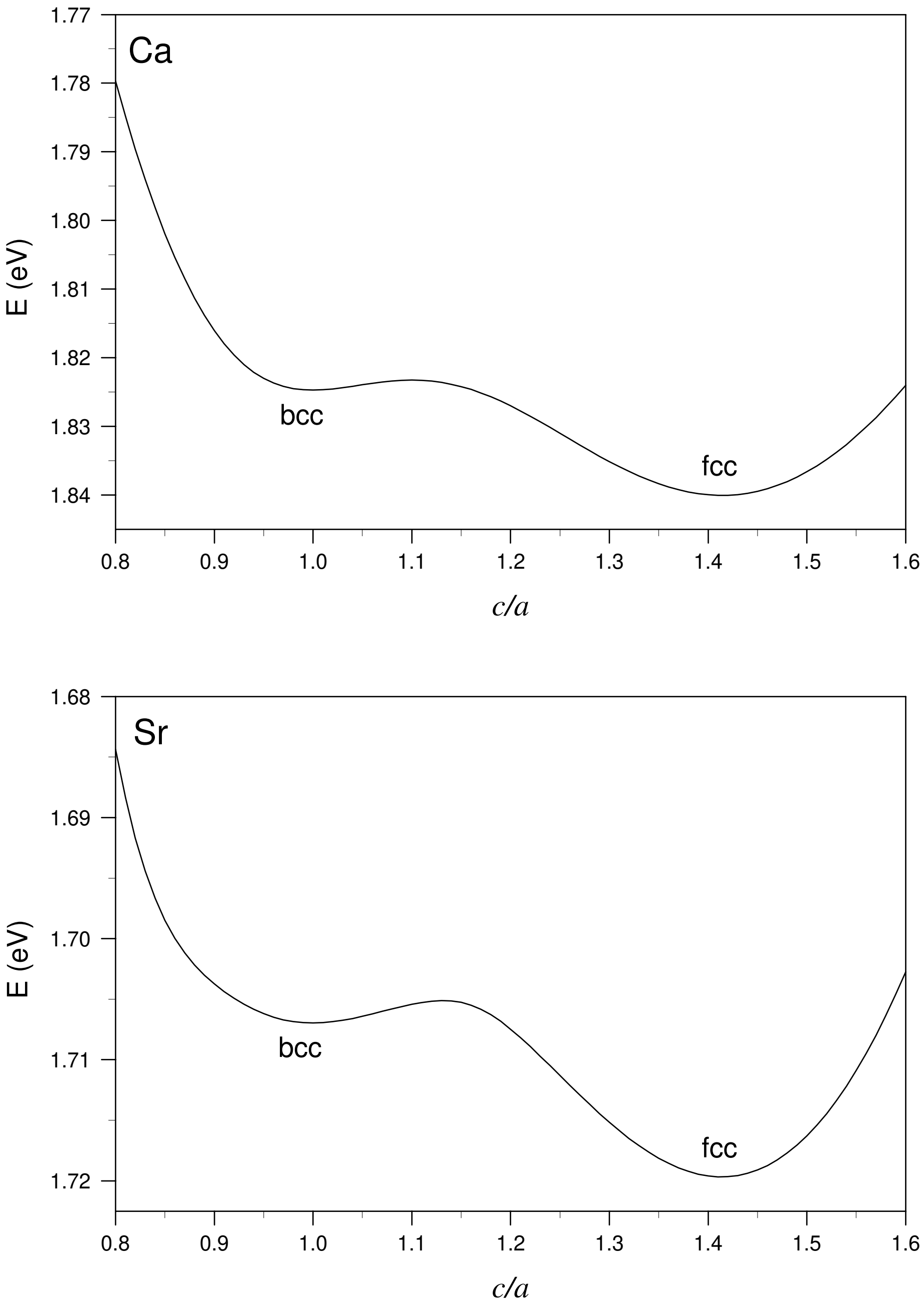

Figure 4: Variation of cohesive energy (E) with c/a ratio, along the Bain deformation path, for Ca and Sr.

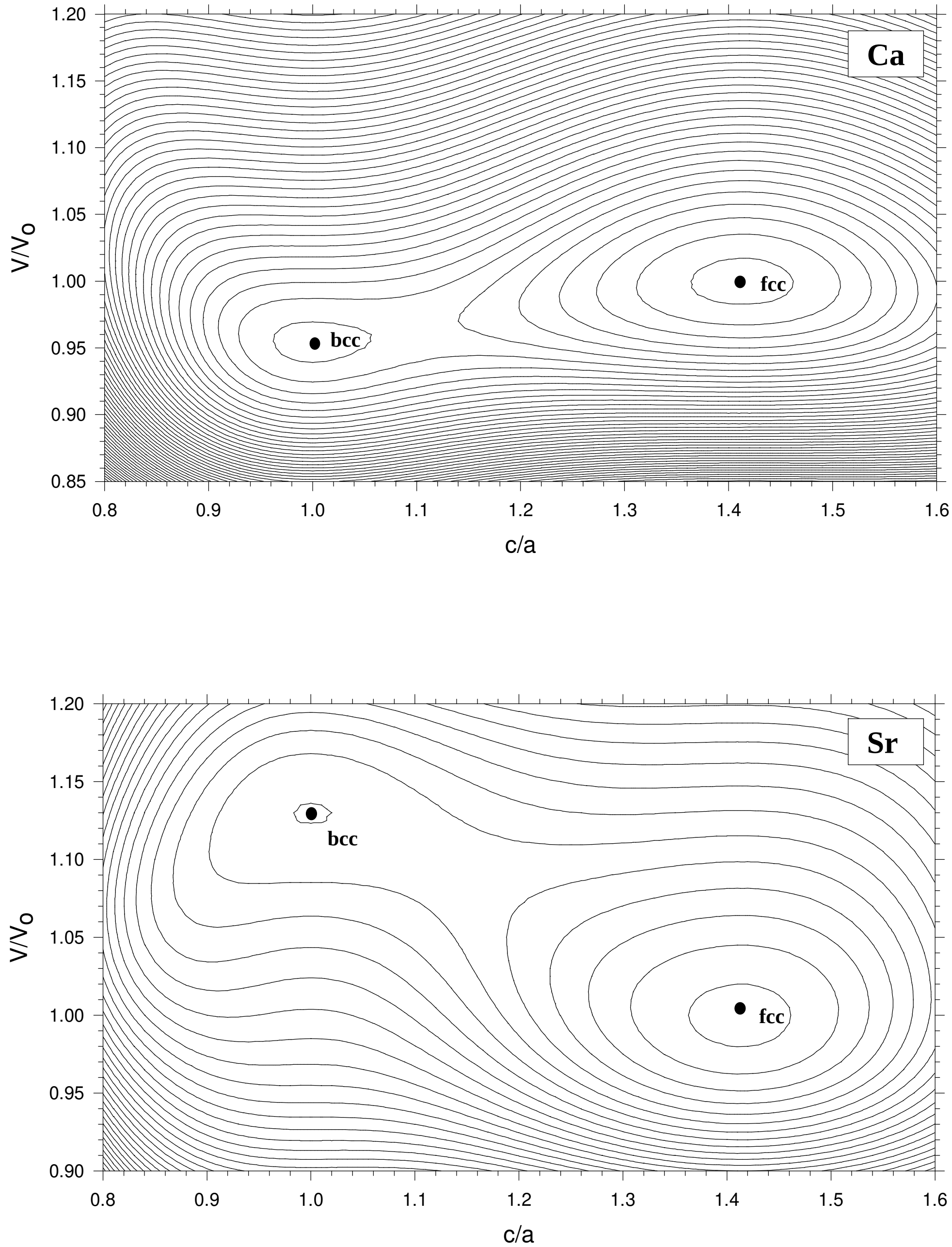

Figure 5: Contour plots of the potential-energy surface for centred tetragonal Ca and Sr as a function of c/a and the reduced volume V/V_0. The contour spacing in both cases is 0.003 eV

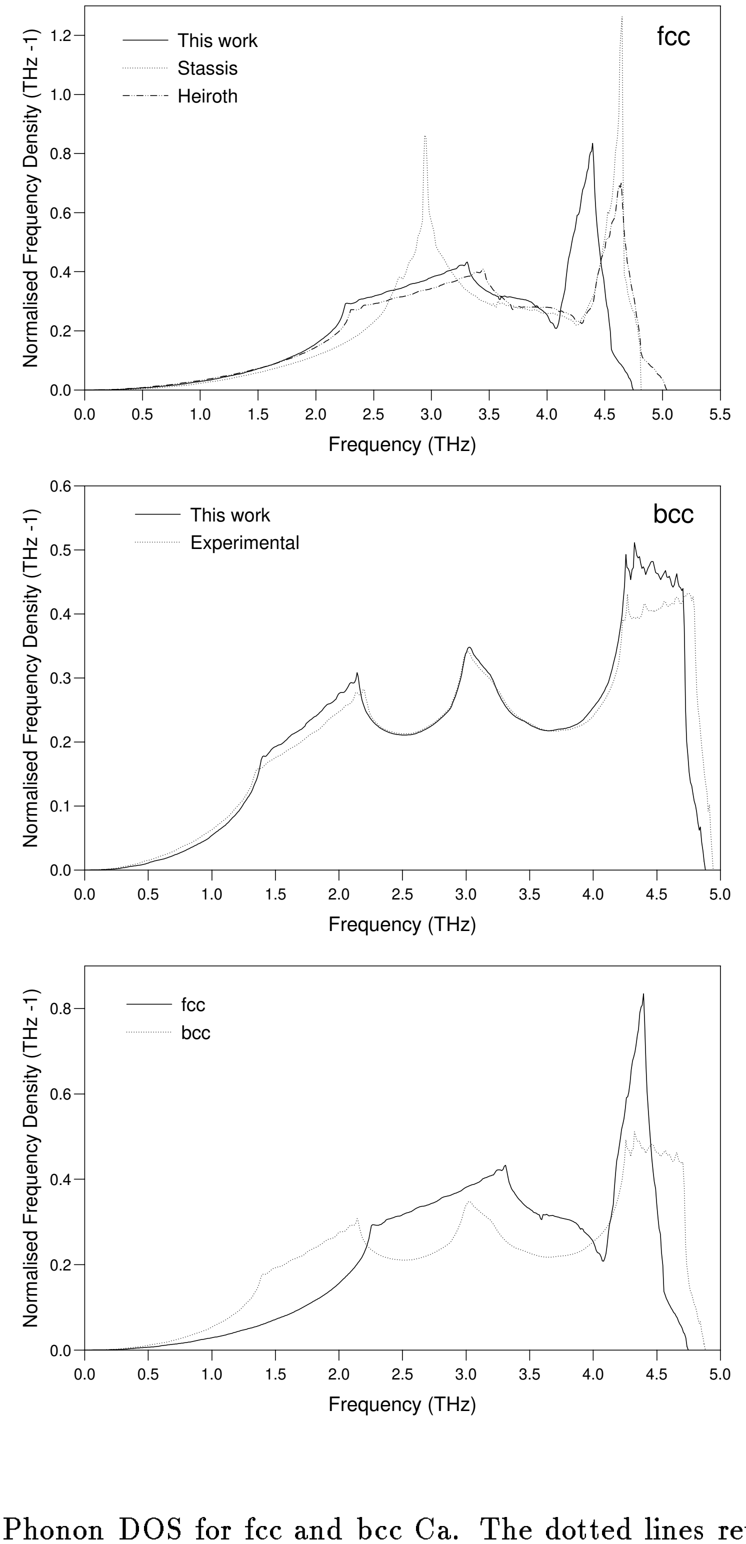

Figure 6: Phonon DOS for fcc and bcc Ca. The dotted lines represent the DOS calculated from experimental force constants.

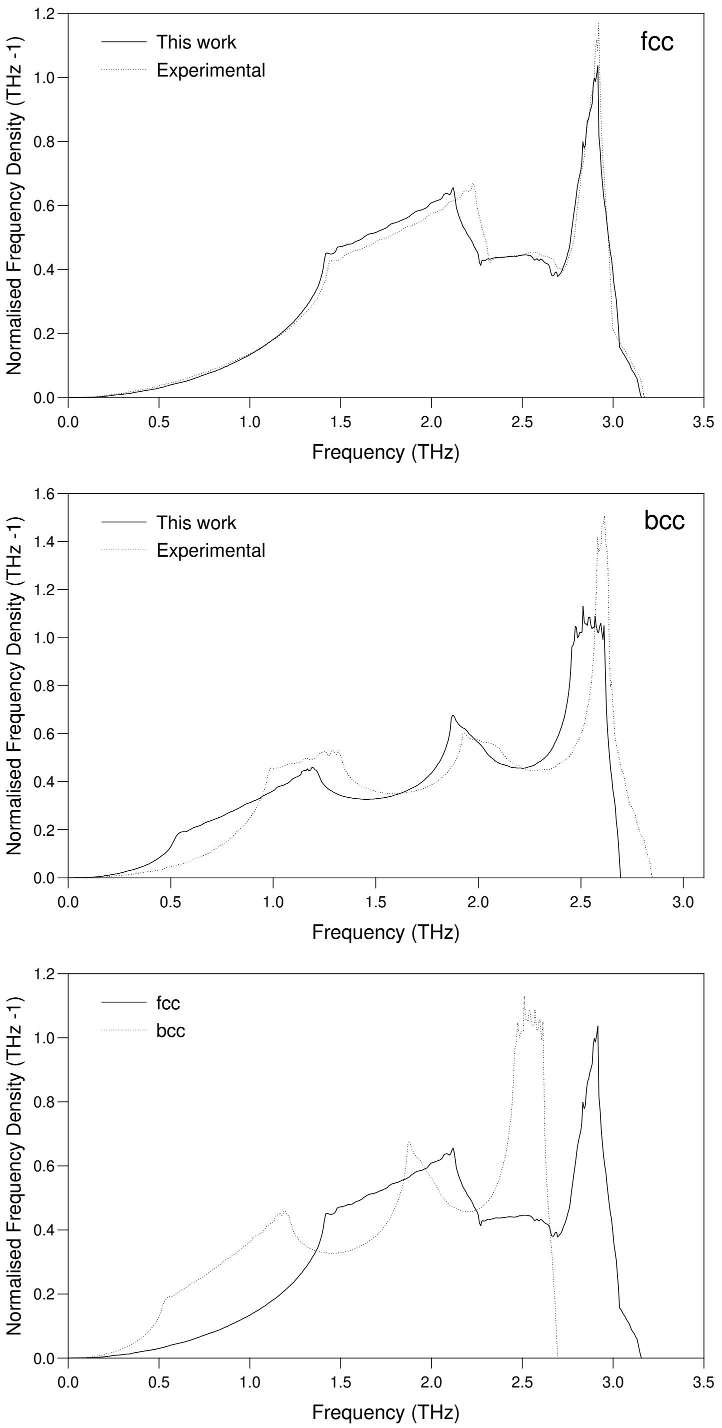

Figure 7: Phonon DOS for fcc and bcc Sr. The dotted lines represent the DOS calculated from experimental force constants.

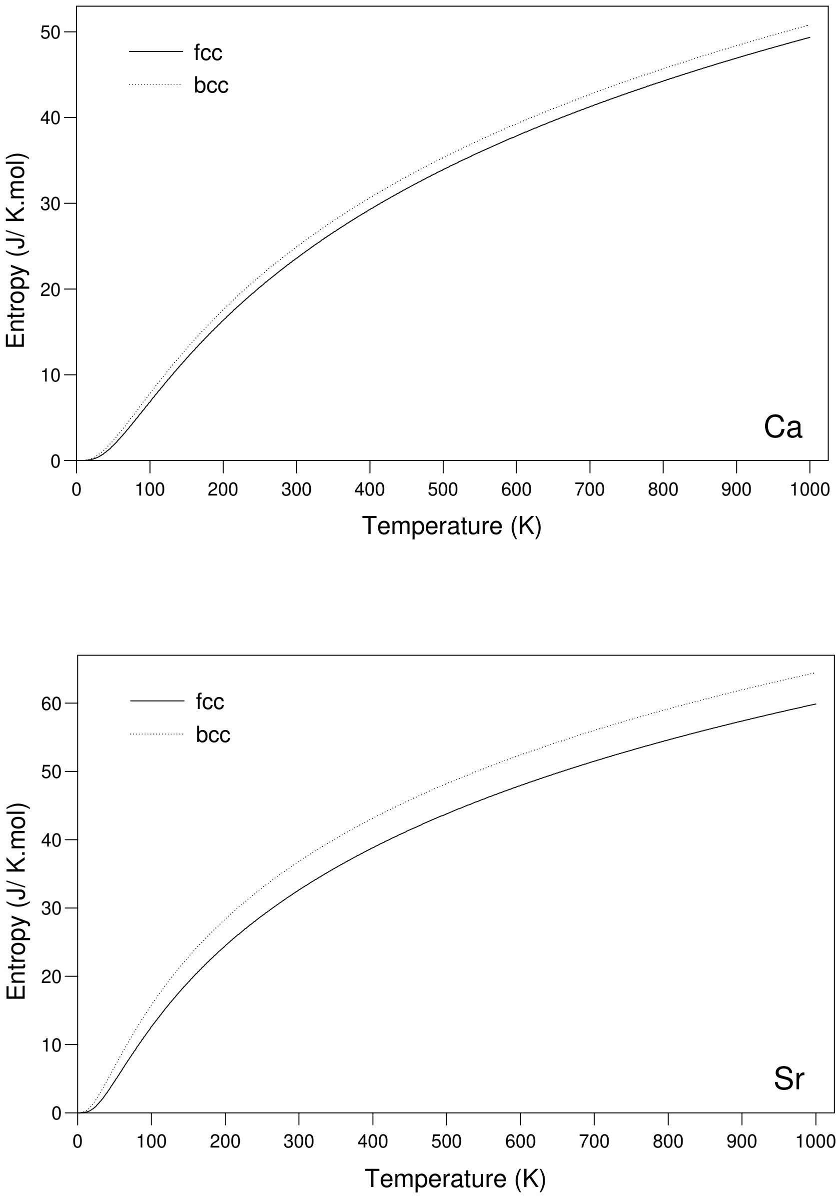

Figure 8: Variation of vibrational entropy with temperature for fcc and bcc Ca and Sr.